Journal of Quantitative Spectroscopy & Radiative Transfer 113 (2012) 991–1003

Contents lists available at SciVerse ScienceDirect

Journal of Quantitative Spectroscopy & Radiative Transfer

journal homepage: www.elsevier.com/locate/jqsrt

Semiclassical calculations of half-widths and line shifts for transitions in the 30012←00001 and 30013←00001 bands of CO_2 II: Collisions with O_2 and air

Julien Lamouroux [a,b], Robert R. Gamache [a,b,*], Anne L. Laraia [a,b], Jean-Michel Hartmann [c], Christian Boulet [d]

[a] University of Massachusetts School of Marine Sciences, University of Massachusetts Lowell, 1 University Avenue, Lowell, MA 01854-5045, USA
[b] Department of Environmental, Earth, and Atmospheric Sciences, University of Massachusetts Lowell, 1 University Avenue, Lowell, MA 01854-5045, USA
[c] Laboratoire Interuniversitaire des Systèmes Atmosphériques, CNRS (UMR 7583), Université Paris Est Créteil, Université Paris Diderot, Institut Pierre-Simon Laplace, Université Paris Est Créteil, 94010 Créteil Cedex, France
[d] Institut des Sciences Moléculaires d'Orsay (ISMO;UMR 8214), CNRS, Univ. Paris-Sud, Bat. 350, Campus d'ORSAY, 91405 ORSAY Cedex, France

ARTICLE INFO

Available online 18 February 2012

Keywords:
Carbon dioxide
CO_2–O_2
CO_2-air
Half-widths
Temperature dependence
Line-shifts

ABSTRACT

The complex Robert–Bonamy (CRB) formalism was used to calculate the half-width, its temperature dependence, and the line shift for CO_2 for transitions in the 30012←00001 and 30013←00001 bands with O_2 as the perturbing gas. The calculations were done for rotational quantum numbers from $J=0$ to $J=120$ with no ad hoc scaling of the line shape equations. The intermolecular potential parameters are adjusted on accurate experimental measurements of the half-widths, its temperature dependence, and the pressure-induced line shifts so that a single intermolecular potential reproduces all three parameters. Using the results of this work and previous results for N_2-broadening, air-broadening line shape parameters were also determined. The comparison of the CRB calculations with the experimental data available in the literature for the three line shape coefficients demonstrates the quality of the present calculations for the both bands under study.

1. Introduction

In a recent study [1], hereafter called Part I, calculations of the half-widths, its temperature dependence, and the line shifts for N_2 broadening of CO_2 were done using the Complex Robert–Bonamy (CRB) formalism. The calculations considered two bands belonging to the Fermi tetrad, $2\nu_1+2\nu_2+\nu_3$ and $\nu_1+4\nu_2+\nu_3$ (or 30012←00001 and 30013←00001, respectively, see HITRAN [2] or Toth et al. [3] for details) in the 1.6 μm spectral region, which is extensively used for remote sensing of the Earth's atmosphere. For example, the successor of the Orbiting Carbon Observatory mission [4] (lost in 2009 due to a launch failure), OCO-2 [5], aims at determining the local sources and sinks of CO_2 with a very high precision (0.3%). The Japanese Greenhouse Gases Observatory Satellite (GOSAT) [6], launched in early 2009, and the Carbon Monitoring Satellite (CarbonSat) [7], one of two candidates to be launch in 2018, also use the 1.6 μm region to measure and better understand the carbon dioxide variations in the Earth's atmosphere. This region and other spectral regions are used for the remote sensing of CO_2-rich planetary atmospheres such as Venus and Mars, for example the Visible and InfraRed Thermal Imaging Spectrometer (VIRTIS) [8] onboard the Venus Express, the Ultraviolet and

* Corresponding author at: Department of Environmental, Earth, and Atmospheric Sciences, University of Massachusetts Lowell, 1 University Avenue, Lowell, MA 01854-5045. Tel.: +1 978 934 3904; fax: +1 978 934 3069.
E-mail address: Robert_Gamache@uml.edu (R.R. Gamache).

0022-4073/$ - see front matter © 2012 Elsevier Ltd. All rights reserved.
doi:10.1016/j.jqsrt.2012.02.015

Infrared Atmospheric Spectrometer (SPICAM) [9] onboard the Mars Express ESA missions, and the Mars Climate Sounder (MCS) [10] onboard the Mars Reconnaissance Orbiter satellite. These high-resolution spectrometers, and a number of ground-based network as the Total Carbon Column Observatory Network [11], put very high constraints on the spectroscopic data, especially for the line shape parameters for CO_2.

A summary of previous calculations was given in Part I. The calculations described in Part I are based on the complex implementation of Robert–Bonamy (RB) theory [12]. The RB model (i) eliminates the awkward cutoff procedure present in the earlier theories [13–21] by use of linked-cluster techniques and the cumulant expansion [22], (ii) introduces a short-range atom–atom intermolecular potential, essential for a proper description of pressure broadening [23–26]. The complex implementation (CRB) [27,28] allows the determination of the half-width and the line shift from a single calculation. The effect of the imaginary component has been shown to be important for several systems [28,29] including CO_2–N_2 [1]. The calculations in Part I were done for rotational transitions from $J=0$ up to $J=120$ (where J is the lower state rotational quantum number) and yield a coherent set of pressure broadening and pressure-induced shifting coefficients, which are important for calculations of spectra.

It is important to emphasize that the complex Robert–Bonamy calculations were done by fitting the half-widths, their temperature dependence, and the line shifts simultaneously. The study done for CO_2–N_2 in Part I exposed several features of CO_2 as the absorbing molecule and in particular the strong dependence of the line shape parameters on the intermolecular potential. It was demonstrated that in order to reach the needs of the remote sensing and spectroscopic communities, the calculations must (i) include the imaginary component, (ii) consider a high-order expansion of the intermolecular potential and (iii) describe the collisions dynamics using Hamilton's equations [30] since the parabolic trajectory model yields unphysical results.

This study is the second in a series about CRB calculations of the half-width, its temperature dependence, and the line shift for foreign and self-broadening of CO_2 in the $30012 \leftarrow 00001$ and $30013 \leftarrow 00001$ bands. Here calculations are reported for O_2 as the collision partner and, using the CO_2–N_2 calculations reported in Part I, air-broadened half-widths and air induced line shifts are determined. The comparison of the calculations with measurements available in the literature demonstrates the quality of the present calculations for the both bands and collision partners considered here.

2. Complex Robert–Bonamy formalism

The calculations employ the complex Robert–Bonamy formalism (CRB), which was described in detail in Part I; hence only the main features are given here. In the CRB approach, the half-width, γ, and line shift, δ, of a rovibrational transition $f \leftarrow i$ are obtained from the real and imaginary parts, respectively, of a single calculation

$$\gamma_{f\leftarrow i} = \frac{n_2}{2\pi c}\sum_{J_2}\langle J_2|\rho_2|J_2\rangle \int_0^\infty v f(v)\mathrm{d}v \int_0^\infty 2\pi b[1-\cos\{S_1 + \mathrm{Im}(S_2)\}e^{-Re(S_2)}]\mathrm{d}b \quad (1a)$$

$$\delta_{f\leftarrow i} = \frac{n_2}{2\pi c}\sum_{J_2}\langle J_2|\rho_2|J_2\rangle \int_0^\infty v f(v)\mathrm{d}v \int_0^\infty 2\pi b\sin\{S_1 + \mathrm{Im}(S_2)\}e^{-Re(S_2)}\mathrm{d}b \quad (1b)$$

where v is the relative velocity, b is the impact parameter, ρ_2 and n_2 are the density operator (its matrix element yields the relative population) and number density of perturbers. S_1 and S_2 are, respectively, the first and the second order terms in the successive expansion of the Liouville scattering matrix S. S_1 is the (imaginary) isotropic vibrational dephasing term and can be written in terms of the isotropic London dispersion potential. S_1 depends on the change of the polarizability with the vibrational states of CO_2 for a transition $f \leftarrow i$. The S_2 terms are the complex analog of those appearing in the Anderson–Tsao–Curnutte (ATC) theory [13–15]. These terms involve the dynamics of the collision and the associated collision jumps from rovibrational levels involved. The exact forms of these terms can be found in Part I and references therein.

The intermolecular potential used in the calculations is comprised of an electrostatic, an atom–atom, and a London dispersion part. The first part consists of the leading electrostatic components of CO_2–O_2 pair (quadrupole moment of CO_2 with the quadrupole moment of O_2). The atom–atom potential is defined as the sum of pairwise Lennard-Jones 6–12 interactions [31] between atoms of the radiating molecule CO_2 and the perturbing molecule O_2. The heteronuclear atom–atom parameters, ε_{ij} and σ_{ij} (i and j are indices running on the atoms of the radiating and perturbing molecules), are usually constructed from homonuclear ones, ε_{ii} and σ_{ii}, by combination rules [32–35]. The ε_{ij} and σ_{ij} atom–atom parameters are not as well known as the other parameters as their values can differ significantly depending of the method used to derive them. Their adjustment on reliable experimental data has been shown to result in a better agreement with measurements [36–38]. The atom–atom potential is mapped using the tensorial formulation of Gray and Gubbins [39] from the atom–atom distance, r_{ij}, to the center of mass separation R using the expansion of Sack [40]. The expansion can be made to any *order* and *rank* using the method developed by Neshyba and Gamache [41]. Following the study of convergence made in Part I for CO_2–N_2, the present study used a potential expanded to 20th *order* and the *rank* for CO_2 and O_2 set to 4, labeled 20 4 4.

In Part I [1] it was demonstrated that the parabolic trajectory model fails to give physical results for CO_2 systems. Hence, the present calculations used a trajectory model based on Hamilton's equations, in which the trajectories are obtained by numerically solving the classical equations of motion for the Hamiltonian formed by the kinetic energy and the isotropic part of the atom–atom potential [30].

Table 1
Spectroscopic constants for the 00001, 30012 and 30013 states of CO_2.

	G_v	B_v	D_v (10^{-6})	H_v (10^{-12})	Ref
00001	0.0000	0.390218949 (36)	0.1334088 (186)	0.01918 (250)	[48]
30012	6347.8509109 (41)	0.3864550696 (153)	0.0983477 (159)	0.5974 (44)	[49]
30013	6227.9165646 (40)	0.3867111479 (144)	0.1717038 (144)	0.10552 (38)	[50]

When possible the molecular constants used in the calculations are fixed at the best-measured values. The polarizability of CO_2, 29.13×10^{-25} cm^3, is taken from Ref. [42] and the ionization potential, 13.77 eV, is from Ref. [43]. The quadrupole moment of O_2, $\Theta_{zz}(O_2)=-0.4\times10^{-26}$ esu, is from Stogryn and Stogryn [44]; the polarizability and the ionization potential of O_2 are 15.8×10^{-25} cm^3 [45] and 12.0603 eV [43], respectively. However, the quadrupole moment of CO_2 was adjusted in a study done for self-broadening of CO_2 [46] and that value is used here; $\Theta_{zz}(CO_2)=-3.698\times10^{-26}$ esu. This value is 8% smaller than the value given by Graham et al. [47] but is roughly at 2σ plus the systematic error reported by Graham et al. The rotational constants B, D, H for CO_2 are taken from Miller and Brown [48] for the ground state, and from Devi et al. [49,50] for the 30012 and 30013 states. For the convenience of the reader, the numerical values are given in Table 1. The rotational constant for O_2, $B=1.4377$ cm^{-1}, is from Huber and Herzberg [51]. The coefficients of the vibrational dependence of the polarizability of CO_2 were determined in part I ($a_1=0.140$, $a_2=0.07$ and $a_3=0.268$) and are used in the present study.

The wavefunctions used to evaluate the reduced matrix elements are developed in Wigner D-matrix basis. The energies are calculated using the standard expression [52] given in terms of the molecular rotation constants given in Table 1.

Finally, the following calculations employ the averaging over the Boltzmann distribution of relative velocities, since the use of the mean relative thermal velocity approximation can introduce uncertainty for some systems [53,54] greater than that required for the spectroscopic and remote sensing communities [55–57].

3. Calculations

Calculations of the half-widths, its temperature dependence, and the line shifts were done for P- and R-branch transitions in the 30012←00001 and 30012←00001 bands of CO_2 for J from 0 to 120 and O_2 as the perturbing gas.

The procedure used for the present calculations is similar to the one described in the previous study for CO_2–N_2 [1]. The initial values of the atom–atom parameters ε_{OO}, ε_{CO}, σ_{OO}, and σ_{CO} are determined using the combination rules of Hirschfelder et al. [32] with the homonuclear parameters of Bouanich et al. [58]. The initial isotropic parameters used in the trajectory calculations are determined by fitting the isotropic part of the expanded potential to an effective 6–12 Lennard-Jones potential. These parameters are given in Table 2. Fig. 1 shows the comparison of the calculated half-widths and line shifts determined from the initial parameters (labeled Pot0) with the measurements of Devi et al. [59] vs m ($m=-J$ for P-branch transitions and $J+1$ for R-branch transitions). The agreement is not good and more important; the calculated line shape parameters do not reproduce the m-dependence of the measurements. Next, the intermolecular parameters that are not as well known (atom–atom and trajectory parameters) were adjusted to give results that agree with the measurements of Devi et al. [59]. These data have been chosen because coherent sets of measurements from this group are available for CO_2–N_2, CO_2–O_2, CO_2-air and CO_2–CO_2, moreover they are considered among the most extensive and accurate.

Table 2
Initial and final adjusted intermolecular potential parameters.

Parameter	Initial values	Final values	% change
$\Theta_{zz}(CO_2)$ (esu)	-4.02×10^{-26}	-3.698×10^{-26}	−8
ε_{OO}/k (K)	51.73	69.47	34.3
ε_{CO}/k (K)	40.43	40.43	0
σ_{OO} (Å)	3.010	2.951	−1.96
σ_{CO} (Å)	3.285	3.285	0
ε_{traj}/k (K)	120.3	67.12	−44.21
σ_{traj} (Å)	3.983	3.721	−6.57

The adjustment procedure was started using a non-linear least squares procedure, which ran for 12 iterations and was not converging. To proceed, the influence on the line shape parameters due to an increase of 5% of each intermolecular parameter (individually) was studied. The percent difference between these and the 12th iteration calculations were determined as a function of m. From these data, and the initial calculations (Fig. 1), the adjustment of the parameters to generate data that agrees with measurement can be estimated. The final values were then obtained in about 25 iterations by hand. The final values are also given in Table 2. As discussed in our previous work, because the carbon atom is on the center of mass of the carbon dioxide molecule, ε_{CO} and σ_{CO} do not affect the line shape parameters, so they were held fixed.

Using the reported half-widths at 4 temperatures (200, 250, 296 and 350 K), a range more consistent with the measurements and Earth's atmosphere, the temperature dependence exponent n is defined by the standard power law

$$\gamma(T)=\gamma(T_0)\left\{\frac{T_0}{T}\right\}^n \tag{3}$$

where $\gamma(T_0)$ is the half-width at the reference temperature, $T_0=296$ K. Here, the temperature exponent, n, is obtained by a linear least-squares fit of $\ln\{\gamma(T)/\gamma(T_0)\}$ versus $\ln\{T_0/T\}$ using the half-widths calculated at the

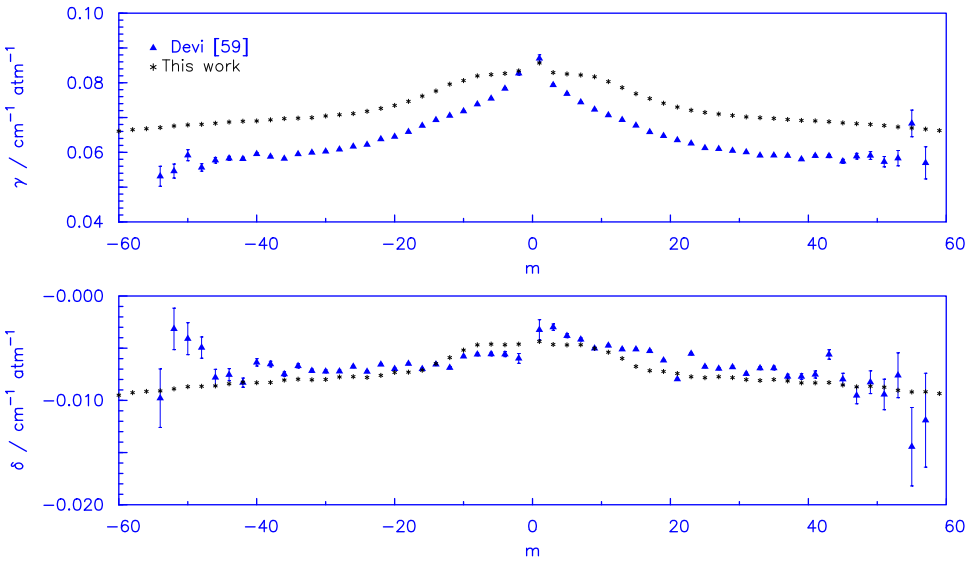

Fig. 1. CO_2–O_2, 30012←00001 band: comparison of initial CRB calculations to the measurements of Devi et al. [59] for the half-width and line shift in $cm^{-1}\,atm^{-1}$ at $T=296$ K. Top panel half-widths versus m, middle panel line shifts versus m.

four temperatures listed above. Comparing the least-squares value of n to those determined by using any 2 points of the four temperatures considered (This generates six 2-point values of n.) the uncertainty of the calculated temperature exponents can be determined by the maximum difference between the least squares value and the six 2-point values. This procedure yields the maximum error in n, however, given the nature of the data and other uncertainties it is thought to be more reasonable than a statistical value taken from the fit.

The half-widths and line shifts were calculated at each temperature for transitions in the 30012←00001 and 30013←00001 bands for the CO_2-air collision system using the calculations reported in our previous study for CO_2–N_2 [1], and the present calculations for CO_2–O_2, using the standard formulae

$$\gamma_{Air} = 0.79*\gamma_{N_2} + 0.21*\gamma_{O_2}$$
$$\delta_{Air} = 0.79*\delta_{N_2} + 0.21*\delta_{O_2} \quad (4)$$

The temperature dependence of the air-broadened half-widths for each transition is then determined by Eq. (3) for the 200–350 K range.

4. Results

4.1. Results for CO_2–O_2

With the intermolecular potential parameters determined, the calculations of half-widths and line shifts for CO_2–O_2 in the 30012←00001 and 30013←00001 bands were made at 13 temperatures; 75, 80, 90, 100, 125, 150, 200, 250, 296, 350, 400, 500, 700 K. It is difficult to determine the uncertainty in the calculated half-widths and line shifts. Comparison with the measurements suggests that the half-widths are known with an uncertainty of about 1% and the line shifts are known with an uncertainty of $\pm 0.0009\,cm^{-1}\,atm^{-1}$. The calculated results for the 30012←00001 and 30013←00001 bands are identical within the stated uncertainties so only the data for the 30012←00001 band are given in Table 3. Presented are the half-widths γ ($cm^{-1}\,atm^{-1}$), its temperature dependence n with its uncertainty, and line shifts δ ($cm^{-1}\,atm^{-1}$) for $-120 \le m \le 121$. However, both bands are compared with measurement.

The comparisons of the calculations with measurements from the literature are shown in the Figs. 2 and 3 for the transitions in the 30012←00001 and 30013←00001 bands, respectively. The top panel of the figures shows the half-widths in $cm^{-1}\,atm^{-1}$ versus m, the middle panel shows the line shifts in $cm^{-1}\,atm^{-1}$ versus m, and the bottom panel shows the temperature dependence of the half-width versus m. All the measured points have 2-sigma error bars. Because there are no measurements of temperature dependence of the half-width available only the calculations are present in the bottom panel along with a black dash line for the "rule-of-thumb" value for a quadrupole-quadrupole system given by Birnbaum [60], $n=0.75$.

The statistics of the comparison with measurements are given in Table 4 as a function of reference and band. The calculated half-widths agree well with the measurement of Devi et al. [59] with an average percent difference (APD) of 0.06 and a standard deviation (SD) of 2.96% for the 56 transitions in the range P(56)–R(56). For the line shifts, as in part I, the average deviation (AD) between measurement and calculation, $AD = (\sum_{i=1}^{N}(\delta_{meas} - \delta_{calc}))/N$, is given along with the standard deviation of this quantity ($S\tilde{D}$). Comparing with the data of Devi *et al.* gives an average deviation of $0.00022\,cm^{-1}\,atm^{-1}$ and $S\tilde{D} = 0.0016\,cm^{-1}\,atm^{-1}$. If the transitions with high uncertainty, $J \ge 50$, are excluded from the measurements (see Fig. 2) the statistics become −0.04 APD ($0.00032\,cm^{-1}\,atm^{-1}$ AD) and 1.59% SD ($0.00089\,cm^{-1}\,atm^{-1}$ $S\tilde{D}$) for the half-widths (line shifts) for the 49

Table 3
Half-width, its temperature dependence, and line shift from the CRB calculations for the CO_2–O_2 system: CO_2 transitions for $-120 \le m \le 121$ in the 30012←00001 band. The half-widths and line shifts are given in $cm^{-1}\ atm^{-1}$ at $T=296$ K.

m	30012←00001				30012←00001		
	γ	n	δ		γ	n	δ
−120	0.0483	0.606 ± 0.031	−0.0121	1	0.0825	0.734 ± 0.015	−0.0041
−118	0.0486	0.610 ± 0.032	−0.0119	3	0.0790	0.736 ± 0.014	−0.0044
−116	0.0489	0.614 ± 0.032	−0.0118	5	0.0778	0.723 ± 0.013	−0.0045
−114	0.0492	0.618 ± 0.033	−0.0116	7	0.0762	0.705 ± 0.011	−0.0047
−112	0.0495	0.621 ± 0.034	−0.0115	9	0.0743	0.686 ± 0.010	−0.0050
−110	0.0498	0.625 ± 0.034	−0.0114	11	0.0723	0.670 ± 0.011	−0.0055
−108	0.0501	0.628 ± 0.034	−0.0112	13	0.0704	0.664 ± 0.015	−0.0058
−106	0.0504	0.631 ± 0.035	−0.0111	15	0.0684	0.662 ± 0.020	−0.0061
−104	0.0507	0.634 ± 0.035	−0.0110	17	0.0665	0.662 ± 0.025	−0.0065
−102	0.0510	0.637 ± 0.035	−0.0108	19	0.0647	0.666 ± 0.030	−0.0068
−100	0.0513	0.640 ± 0.035	−0.0107	21	0.0633	0.673 ± 0.035	−0.0070
−98	0.0516	0.643 ± 0.035	−0.0106	23	0.0622	0.682 ± 0.038	−0.0072
−96	0.0519	0.645 ± 0.035	−0.0104	25	0.0613	0.692 ± 0.041	−0.0073
−94	0.0522	0.649 ± 0.035	−0.0103	27	0.0606	0.700 ± 0.042	−0.0074
−92	0.0525	0.651 ± 0.035	−0.0102	29	0.0601	0.708 ± 0.042	−0.0075
−90	0.0528	0.654 ± 0.034	−0.0101	31	0.0597	0.714 ± 0.042	−0.0076
−88	0.0531	0.657 ± 0.034	−0.0099	33	0.0594	0.719 ± 0.041	−0.0076
−86	0.0534	0.660 ± 0.034	−0.0098	35	0.0591	0.722 ± 0.040	−0.0077
−84	0.0537	0.662 ± 0.033	−0.0097	37	0.0589	0.724 ± 0.038	−0.0077
−82	0.0540	0.665 ± 0.033	−0.0096	39	0.0587	0.725 ± 0.037	−0.0077
−80	0.0543	0.668 ± 0.032	−0.0095	41	0.0585	0.725 ± 0.036	−0.0078
−78	0.0545	0.671 ± 0.032	−0.0093	43	0.0584	0.724 ± 0.035	−0.0078
−76	0.0548	0.674 ± 0.032	−0.0092	45	0.0582	0.722 ± 0.034	−0.0079
−74	0.0551	0.677 ± 0.031	−0.0091	47	0.0580	0.720 ± 0.033	−0.0079
−72	0.0554	0.680 ± 0.031	−0.0090	49	0.0579	0.718 ± 0.032	−0.0080
−70	0.0556	0.683 ± 0.031	−0.0089	51	0.0577	0.715 ± 0.031	−0.0081
−68	0.0559	0.687 ± 0.030	−0.0088	53	0.0575	0.712 ± 0.031	−0.0081
−66	0.0561	0.690 ± 0.030	−0.0087	55	0.0573	0.709 ± 0.031	−0.0082
−64	0.0564	0.693 ± 0.030	−0.0086	57	0.0571	0.706 ± 0.030	−0.0083
−62	0.0566	0.697 ± 0.030	−0.0085	59	0.0569	0.703 ± 0.030	−0.0084
−60	0.0568	0.700 ± 0.030	−0.0084	61	0.0567	0.699 ± 0.030	−0.0085
−58	0.0570	0.703 ± 0.030	−0.0083	63	0.0565	0.696 ± 0.030	−0.0086
−56	0.0572	0.707 ± 0.030	−0.0083	65	0.0563	0.693 ± 0.030	−0.0087
−54	0.0574	0.710 ± 0.030	−0.0082	67	0.0560	0.690 ± 0.031	−0.0088
−52	0.0576	0.713 ± 0.031	−0.0081	69	0.0558	0.687 ± 0.031	−0.0089
−50	0.0578	0.716 ± 0.032	−0.0080	71	0.0555	0.683 ± 0.031	−0.0090
−48	0.0580	0.719 ± 0.032	−0.0080	73	0.0553	0.680 ± 0.032	−0.0091
−46	0.0581	0.721 ± 0.033	−0.0079	75	0.0550	0.677 ± 0.032	−0.0092
−44	0.0583	0.723 ± 0.034	−0.0079	77	0.0547	0.674 ± 0.032	−0.0093
−42	0.0584	0.724 ± 0.035	−0.0078	79	0.0544	0.672 ± 0.033	−0.0095
−40	0.0586	0.725 ± 0.036	−0.0078	81	0.0542	0.669 ± 0.033	−0.0096
−38	0.0588	0.724 ± 0.038	−0.0077	83	0.0539	0.666 ± 0.034	−0.0097
−36	0.0590	0.723 ± 0.039	−0.0077	85	0.0536	0.664 ± 0.034	−0.0098
−34	0.0592	0.721 ± 0.040	−0.0076	87	0.0533	0.661 ± 0.035	−0.0100
−32	0.0595	0.717 ± 0.041	−0.0076	89	0.0530	0.658 ± 0.035	−0.0101
−30	0.0599	0.711 ± 0.042	−0.0075	91	0.0527	0.656 ± 0.035	−0.0102
−28	0.0603	0.704 ± 0.042	−0.0075	93	0.0524	0.653 ± 0.036	−0.0104
−26	0.0609	0.696 ± 0.041	−0.0074	95	0.0522	0.651 ± 0.036	−0.0105
−24	0.0617	0.687 ± 0.040	−0.0073	97	0.0519	0.648 ± 0.036	−0.0106
−22	0.0627	0.677 ± 0.037	−0.0071	99	0.0516	0.646 ± 0.036	−0.0108
−20	0.0640	0.669 ± 0.033	−0.0070	101	0.0513	0.643 ± 0.036	−0.0109
−18	0.0656	0.664 ± 0.028	−0.0067	103	0.0510	0.640 ± 0.036	−0.0111
−16	0.0674	0.662 ± 0.022	−0.0064	105	0.0507	0.638 ± 0.036	−0.0112
−14	0.0694	0.663 ± 0.017	−0.0061	107	0.0504	0.635 ± 0.036	−0.0113
−12	0.0713	0.665 ± 0.012	−0.0058	109	0.0501	0.632 ± 0.036	−0.0115
−10	0.0733	0.677 ± 0.010	−0.0054	111	0.0498	0.629 ± 0.035	−0.0116
−8	0.0754	0.696 ± 0.011	−0.0050	113	0.0495	0.625 ± 0.035	−0.0118
−6	0.0771	0.716 ± 0.012	−0.0048	115	0.0492	0.622 ± 0.035	−0.0119
−4	0.0785	0.731 ± 0.014	−0.0046	117	0.0489	0.619 ± 0.034	−0.0121
−2	0.0798	0.739 ± 0.015	−0.0044	119	0.0486	0.615 ± 0.033	−0.0122
				121	0.0483	0.611 ± 0.033	−0.0124

remaining transitions. The agreement with the γ and δ data of De Rosa et al. [61] is not as good; see Fig. 2 or Table 4. However the measured values are randomly distributed as a function of m whereas all other references present smooth variations within the experimental uncertainty. The agreement between the half-widths measured by Li et al. [62] is

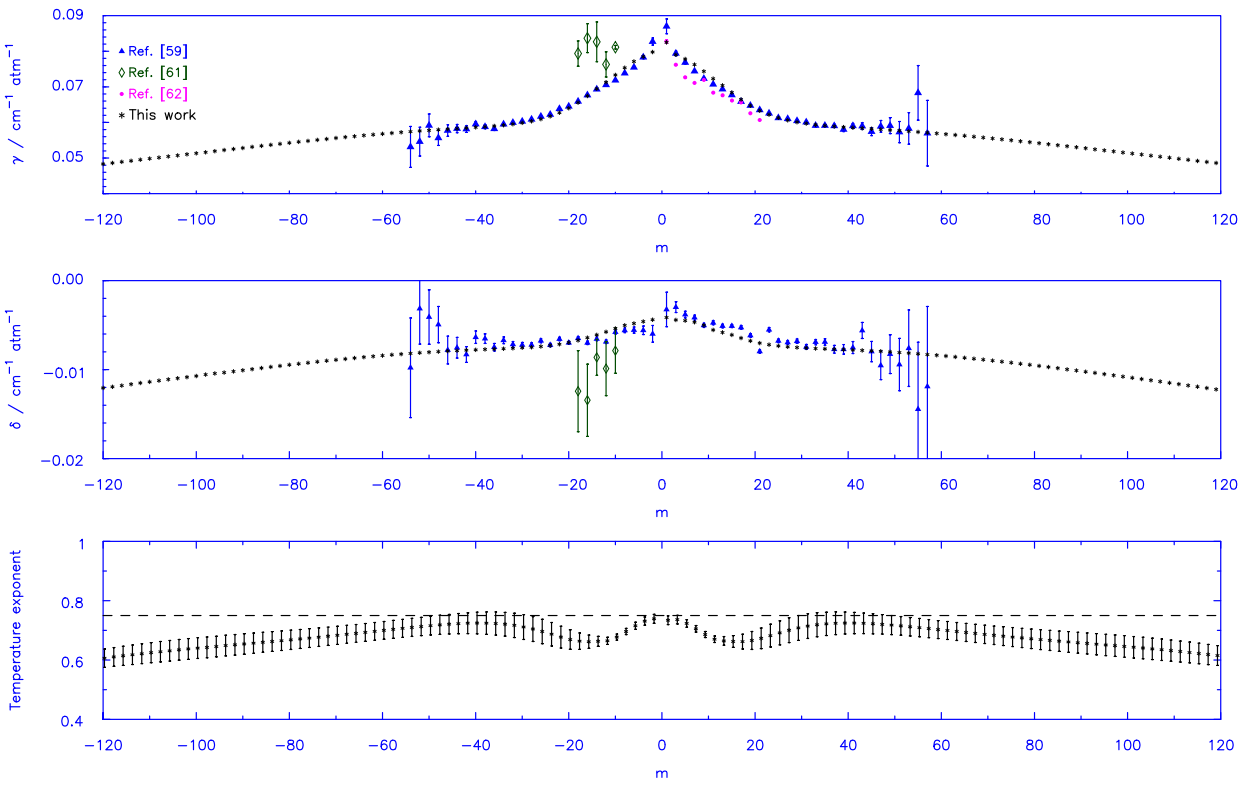

Fig. 2. Final CRB calculations for transitions in the 30012←00001 band of CO_2 broadened by O_2 (at $T=296$ K) and measurements versus m. Top panel half-widths (in $cm^{-1}\,atm^{-1}$) versus m, middle panel line shifts (in $cm^{-1}\,atm^{-1}$) versus m, bottom panel temperature exponent of the half-widths versus m.

good (SD=2.24%), but they are about 3.94% lower in average than our calculations and the other measurements.

The comparison of the calculations and measurements for the 30013←00001 band is shown in Fig. 3, in the same format as Fig. 2. The statistics of the comparison are reported in Table 4. For the half-widths, the agreement between the CRB calculations with the measurements of Devi et al. is similar to the values reported for the 30012←00001 band with an APD of −0.81 and a SD of 2.72%. This agreement for the line shifts is not as good with an AD of $-0.00054\,cm^{-1}\,atm^{-1}$ and a $S\tilde{D}$ of $0.00178\,cm^{-1}\,atm^{-1}$. These high values can be explained by the consideration of the high J transitions from 50 to 56 that have high uncertainty (see Fig. 3). For the 49 transitions from P(48) to R(48), the statistics are APD=−0.81 and SD=1.52% for the half-widths and AD=$0.00045\,cm^{-1}\,atm^{-1}$ and a $S\tilde{D}=0.00077\,cm^{-1}\,atm^{-1}$. (i.e., a factor of 2.3 on $S\tilde{D}$). The agreement with the measurements of Nakamichi et al. [63] is good (see Table 4). Comparison with the measurements of Hikida and Yamada [64] gives an average percent difference of −3.96 and a standard deviation of 3.23%. However these measurements were performed using a Galatry rather than a Voigt profile. The agreement with the measurements of Pouchet et al. [65] give a APD of −4.07 and SD of 1.85%.

The role of the imaginary components of the CRB formalism on the O_2-broadened half-widths and their temperature dependence was investigated for the R-branch transitions in the 30012←00001 band. Calculations were made using the real part of Eq. (1), (RRB), and the half-widths and its temperature dependence were compared with the CRB calculations discussed above. In Fig. 4, the average percent difference and the maximum percent difference between the half-widths calculated with the CRB and RRB formalism are plotted vs temperature. The average difference reaches about 5% and the maximum difference reaches about 15%. At 296 K the average and maximum differences are about 1% and 3%, respectively. These results imply that the temperature exponents should be different between the two methods of calculation. To study this effect the percent differences between the temperature exponent calculated via the CRB method and the RRB method are plotted versus m in Fig. 5. The percent difference between the two methods of calculations increase as a function of m starting near zero for small $|m|$ and increasing with a somewhat parabolic shape to about 10% for $m\sim120$. The curve is asymmetrical in $\pm m$ with the R-branch lines going to about a 10% difference and the P-branch lines to about 9%. The effect of the imaginary terms for O_2-broadening is somewhat stronger that what was observed for N_2-broadening [1]. These studies clearly demonstrate than the imaginary components must be included in the calculations in order to reach the uncertainty requirements of current and future satellite missions.

4.2. Results for CO_2-air

The complex Robert–Bonamy calculations of the half-widths γ (in $cm^{-1}\,atm^{-1}$), its temperature dependence, n, and line shifts δ (in $cm^{-1}\,atm^{-1}$) are given in Table 5 for

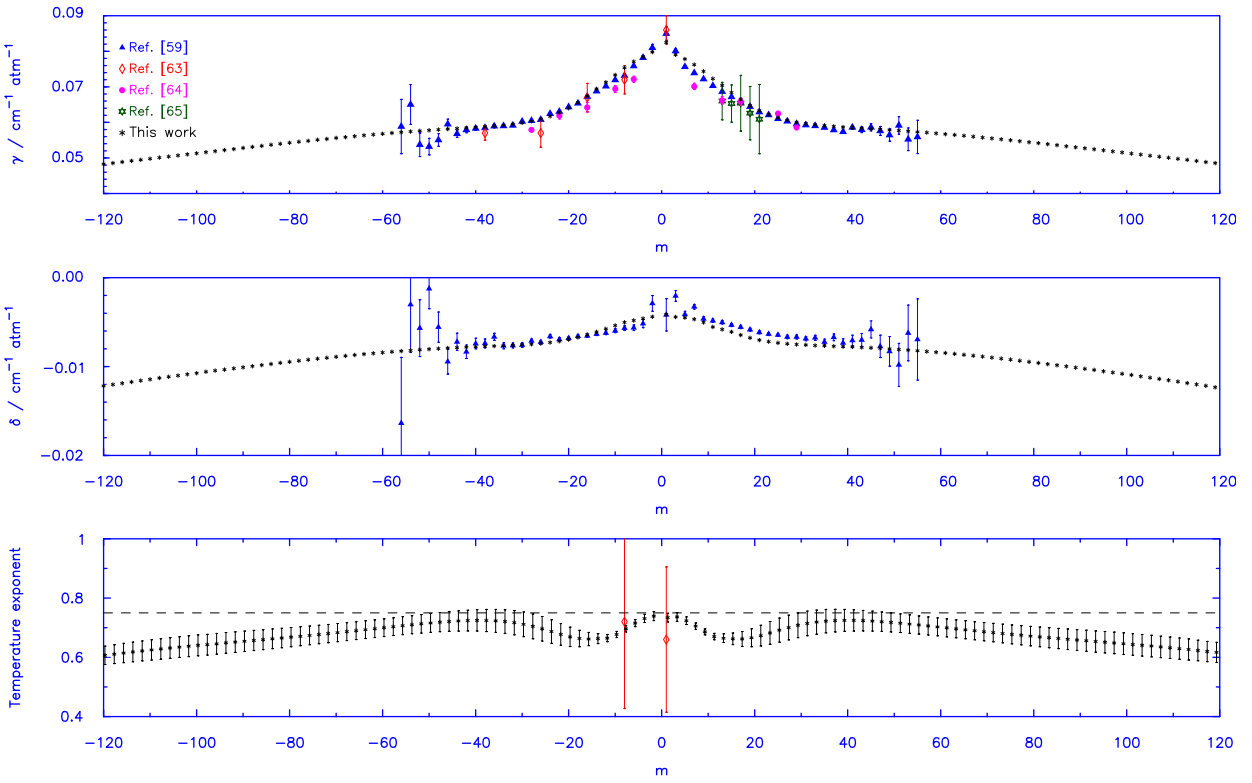

Fig. 3. Final CRB calculations for transitions in the 30013←00001 band of CO_2 broadened by O_2 (at $T=296$ K) and measurements versus m. Top panel half-widths (in $cm^{-1}\,atm^{-1}$) versus m, middle panel line shifts (in $cm^{-1}\,atm^{-1}$) versus m, bottom panel temperature exponent of the half-widths versus m.

Table 4
Statistics for the comparison of the calculations to measurement for CO_2–O_2.

Parameter	Reference	No. of data	APD	SD
30012←00001				
γ	[59]	56	0.06	2.96
	[61]	5	13.78	5.44
	[62]	11	−3.94	2.24
	Reference	No. of data	AD†	$S\tilde{D}$†
δ	[59]	56	0.00022	0.0016
	[61]	5	−0.0044	0.0020
30013←00001				
γ	[59]	56	−0.81	2.72
	[65]	5	−4.07	1.85
	[63]	5	−2.26	4.21
	[64]	10	−3.96	3.23
n	[63]	2	−3.96	–
	Reference	No. of data	AD†	$S\tilde{D}$†
δ	[59]	56	0.00054	0.0018

† see text for definitions of AD and $S\tilde{D}$.

air-broadening for P- and R-branch transitions from $J=0$ to $J=120$ in the 30012←00001 band. As in the case of O_2-broadening the results for the 30012←00001 and 30013←00001 bands are identical to within the error estimates, which for air-broadening are 1% on the half-widths and $\pm 0.0008\ cm^{-1}\,atm^{-1}$ for the line shifts. The CO_2-air half-width and line shift were derived from CO_2–N_2 and CO_2–O_2 parameters using Eq. (4) at each temperature of the study, from which the temperature dependence of the half-widths were determined using Eq. (3). The values are plotted in Fig. 6 for the 30012←00001 band and in Fig. 7 for the 30013←00001 band in the same format as Fig. 2. The CO_2-air measurements plotted in Fig. 6 are those of Devi et al. [49], Li et al. [66], Long et al. [67], Toth et al. [68], Predoi-Cross et al. [69], and Predoi-Cross et al. [70]. Also plotted are CO_2-air parameters derived from N_2 and O_2 buffer gas measurements by Li et al. [62] and by De Rosa et al. [61]. Note that the study of Predoi-Cross et al. [70] reports measurements determined using a Speed-Dependent Voigt (SDV) profile and a Voigt profile. They are similar to each other and only the Voigt profile results for γ and δ are plotted in Figs. 6 and 7. The only direct measurements of the temperature dependence of air-broadened half-widths for the bands under study was done by Predoi-Cross et al. [69] using a SDV profile.

For the 30012←00001 band, the agreement of the CRB calculations with the measurements of Devi et al. for the CO_2-air-system is excellent; APD = −0.10 and SD = 1.27% for the half-widths and AD = 0.00063 $cm^{-1}\,atm^{-1}$ and $S\tilde{D}=0.00052\ cm^{-1}\,atm^{-1}$ for the pressure-induced line shifts. The magnitude of the calculated shifts are larger than those of the measurements; a fact also observed in the previous study for CO_2–N_2 [1] and for the CO_2–O_2 calculations (see above). However the good agreement confirms the coherence of the calculations and the measurements of Devi et al. for CO_2–N_2, CO_2–O_2 and CO_2-air.

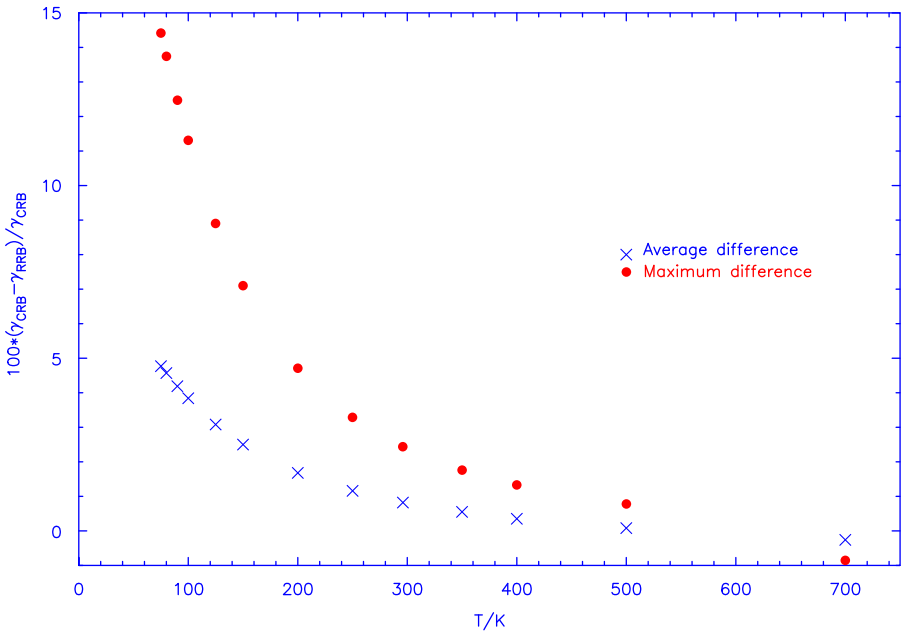

Fig. 4. Effect of the imaginary terms: average percent difference (CRB-RRB) and maximum percent difference for the transitions in the 30012←00001 band versus T(K).

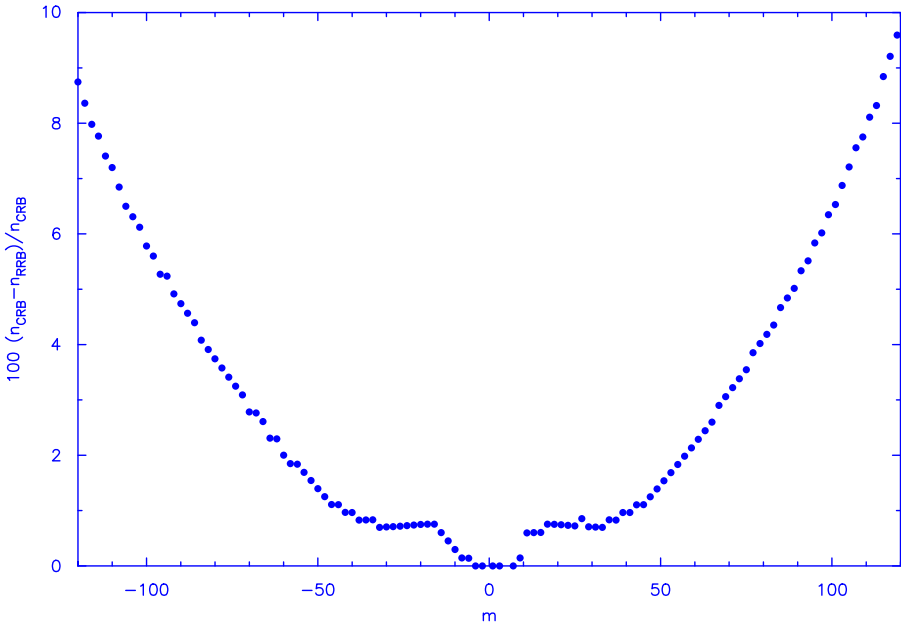

Fig. 5. Effect of the imaginary terms on the temperature dependence: percent change n_{CRB}–n_{RRB} versus m for the transitions in the 30012←00001 band.

The statistics of the comparison of the CRB calculations with measurements are given in Table 6. The agreement of the calculations with the measurements of Toth et al. [68] is very good for both the half-widths and pressure-induced line shifts. The calculations also show good agreement with the measurements of Predoi-Cross et al. [69] for the half-widths and their temperature dependence. For the line shifts compared with Predoi-Cross et al., the average deviation is 0.00080 cm^{-1} atm^{-1} with $S\tilde{D} = 0.00118$ cm^{-1} atm^{-1}. However, the value of the line shift for the $R(50)$ transition (-0.00062 cm^{-1} atm^{-1}) in the Table 4 of Predoi-Cross et al. [69] is unusually small in magnitude and does not follow the trend of the other data. Removing this transition of the comparison gives an average deviation of 0.00068 cm^{-1} atm^{-1} with $S\tilde{D} =$ 0.00080 cm^{-1} atm^{-1}. Agreement with the works of Li et al. is not as good, 4–6%, however their measurements do not agree with the other measurements. The half-width given by Long et al. [67] for the $R(16)$ transition is 2.21% lower than the calculated value, however this difference is

Table 5
Half-width, its temperature dependence, and line shift from the CRB calculations for the CO_2-air system: CO_2 transitions for $-120 \le m \le 121$ in the 30012←00001 band. The half-widths and line shifts are given in $cm^{-1}\ atm^{-1}$ at $T=296$ K.

m	γ	n	δ	m	γ	n	δ
−120	0.0553	0.657 ± 0.061	−0.0111	1	0.0927	0.736 ± 0.014	−0.0044
−118	0.0555	0.654 ± 0.061	−0.0110	3	0.0885	0.737 ± 0.014	−0.0047
−116	0.0558	0.651 ± 0.060	−0.0109	5	0.0872	0.722 ± 0.011	−0.0047
−114	0.0560	0.649 ± 0.060	−0.0108	7	0.0854	0.699 ± 0.008	−0.0049
−112	0.0563	0.646 ± 0.059	−0.0107	9	0.0833	0.676 ± 0.007	−0.0052
−110	0.0566	0.644 ± 0.058	−0.0106	11	0.0811	0.659 ± 0.008	−0.0056
−108	0.0569	0.641 ± 0.057	−0.0105	13	0.0791	0.652 ± 0.012	−0.0059
−106	0.0572	0.638 ± 0.055	−0.0104	15	0.0771	0.650 ± 0.017	−0.0062
−104	0.0576	0.635 ± 0.054	−0.0103	17	0.0752	0.652 ± 0.021	−0.0065
−102	0.0579	0.633 ± 0.052	−0.0102	19	0.0736	0.659 ± 0.027	−0.0067
−100	0.0582	0.631 ± 0.050	−0.0101	21	0.0723	0.671 ± 0.032	−0.0069
−98	0.0586	0.628 ± 0.048	−0.0100	23	0.0713	0.682 ± 0.035	−0.0070
−96	0.0589	0.626 ± 0.046	−0.0098	25	0.0705	0.692 ± 0.037	−0.0071
−94	0.0593	0.625 ± 0.044	−0.0097	27	0.0699	0.700 ± 0.036	−0.0072
−92	0.0597	0.623 ± 0.041	−0.0096	29	0.0694	0.707 ± 0.036	−0.0073
−90	0.0601	0.622 ± 0.039	−0.0095	31	0.0691	0.714 ± 0.035	−0.0073
−88	0.0604	0.621 ± 0.036	−0.0094	33	0.0689	0.719 ± 0.033	−0.0073
−86	0.0608	0.621 ± 0.034	−0.0093	35	0.0686	0.721 ± 0.031	−0.0073
−84	0.0612	0.621 ± 0.032	−0.0092	37	0.0684	0.720 ± 0.028	−0.0074
−82	0.0617	0.622 ± 0.030	−0.0091	39	0.0683	0.718 ± 0.026	−0.0074
−80	0.0620	0.623 ± 0.027	−0.0090	41	0.0681	0.716 ± 0.023	−0.0074
−78	0.0625	0.625 ± 0.025	−0.0089	43	0.0680	0.714 ± 0.022	−0.0075
−76	0.0629	0.627 ± 0.023	−0.0087	45	0.0679	0.710 ± 0.020	−0.0075
−74	0.0633	0.630 ± 0.021	−0.0086	47	0.0677	0.704 ± 0.018	−0.0075
−72	0.0637	0.633 ± 0.019	−0.0085	49	0.0674	0.698 ± 0.016	−0.0076
−70	0.0641	0.637 ± 0.017	−0.0084	51	0.0672	0.692 ± 0.014	−0.0076
−68	0.0645	0.641 ± 0.016	−0.0083	53	0.0670	0.687 ± 0.014	−0.0077
−66	0.0649	0.646 ± 0.014	−0.0082	55	0.0668	0.682 ± 0.013	−0.0078
−64	0.0652	0.651 ± 0.013	−0.0081	57	0.0665	0.675 ± 0.013	−0.0078
−62	0.0656	0.657 ± 0.013	−0.0080	59	0.0661	0.669 ± 0.013	−0.0079
−60	0.0659	0.662 ± 0.012	−0.0079	61	0.0658	0.663 ± 0.013	−0.0080
−58	0.0662	0.668 ± 0.012	−0.0079	63	0.0655	0.658 ± 0.014	−0.0081
−56	0.0665	0.675 ± 0.012	−0.0078	65	0.0651	0.653 ± 0.015	−0.0082
−54	0.0668	0.682 ± 0.012	−0.0077	67	0.0648	0.648 ± 0.016	−0.0083
−52	0.0671	0.688 ± 0.013	−0.0076	69	0.0644	0.643 ± 0.018	−0.0084
−50	0.0673	0.693 ± 0.014	−0.0076	71	0.0640	0.639 ± 0.019	−0.0085
−48	0.0675	0.699 ± 0.016	−0.0076	73	0.0636	0.636 ± 0.021	−0.0086
−46	0.0677	0.706 ± 0.018	−0.0075	75	0.0632	0.633 ± 0.023	−0.0087
−44	0.0679	0.711 ± 0.020	−0.0075	77	0.0628	0.631 ± 0.025	−0.0089
−42	0.0681	0.715 ± 0.022	−0.0074	79	0.0624	0.629 ± 0.027	−0.0090
−40	0.0682	0.717 ± 0.024	−0.0074	81	0.0620	0.627 ± 0.029	−0.0091
−38	0.0684	0.719 ± 0.027	−0.0074	83	0.0616	0.626 ± 0.031	−0.0092
−36	0.0686	0.721 ± 0.030	−0.0074	85	0.0612	0.626 ± 0.033	−0.0093
−34	0.0688	0.720 ± 0.032	−0.0074	87	0.0608	0.626 ± 0.036	−0.0094
−32	0.0690	0.717 ± 0.034	−0.0073	89	0.0604	0.626 ± 0.038	−0.0096
−30	0.0692	0.710 ± 0.035	−0.0073	91	0.0600	0.627 ± 0.041	−0.0097
−28	0.0696	0.703 ± 0.036	−0.0072	93	0.0596	0.628 ± 0.043	−0.0098
−26	0.0702	0.696 ± 0.037	−0.0072	95	0.0593	0.630 ± 0.045	−0.0099
−24	0.0709	0.687 ± 0.036	−0.0071	97	0.0589	0.631 ± 0.047	−0.0100
−22	0.0718	0.677 ± 0.034	−0.0070	99	0.0586	0.633 ± 0.049	−0.0102
−20	0.0729	0.665 ± 0.029	−0.0068	101	0.0582	0.635 ± 0.051	−0.0103
−18	0.0743	0.655 ± 0.024	−0.0067	103	0.0579	0.638 ± 0.053	−0.0104
−16	0.0761	0.650 ± 0.019	−0.0065	105	0.0575	0.640 ± 0.055	−0.0105
−14	0.0781	0.651 ± 0.014	−0.0062	107	0.0572	0.643 ± 0.056	−0.0106
−12	0.0801	0.654 ± 0.010	−0.0059	109	0.0569	0.646 ± 0.057	−0.0107
−10	0.0822	0.667 ± 0.007	−0.0055	111	0.0566	0.649 ± 0.059	−0.0108
−8	0.0844	0.688 ± 0.007	−0.0053	113	0.0563	0.652 ± 0.060	−0.0109
−6	0.0864	0.712 ± 0.010	−0.0051	115	0.0561	0.654 ± 0.060	−0.0110
−4	0.0879	0.731 ± 0.013	−0.0048	117	0.0558	0.657 ± 0.061	−0.0111
−2	0.0893	0.739 ± 0.014	−0.0046	119	0.0555	0.660 ± 0.062	−0.0112
				121	0.0553	0.662 ± 0.062	−0.0113

expected since a Speed-Dependent model was used in their analysis.

In Fig. 7 the CO_2-air measurements for the 30013←00001 band are from Devi et al. [50], Toth et al. [68], Predoi-Cross et al. [69,70]. Also plotted are CO_2-air parameters derived from N_2 and O_2 buffer gas measurements by Pouchet et al. [65], Hikida and Yamada [64], and Nakamichi et al. [63].

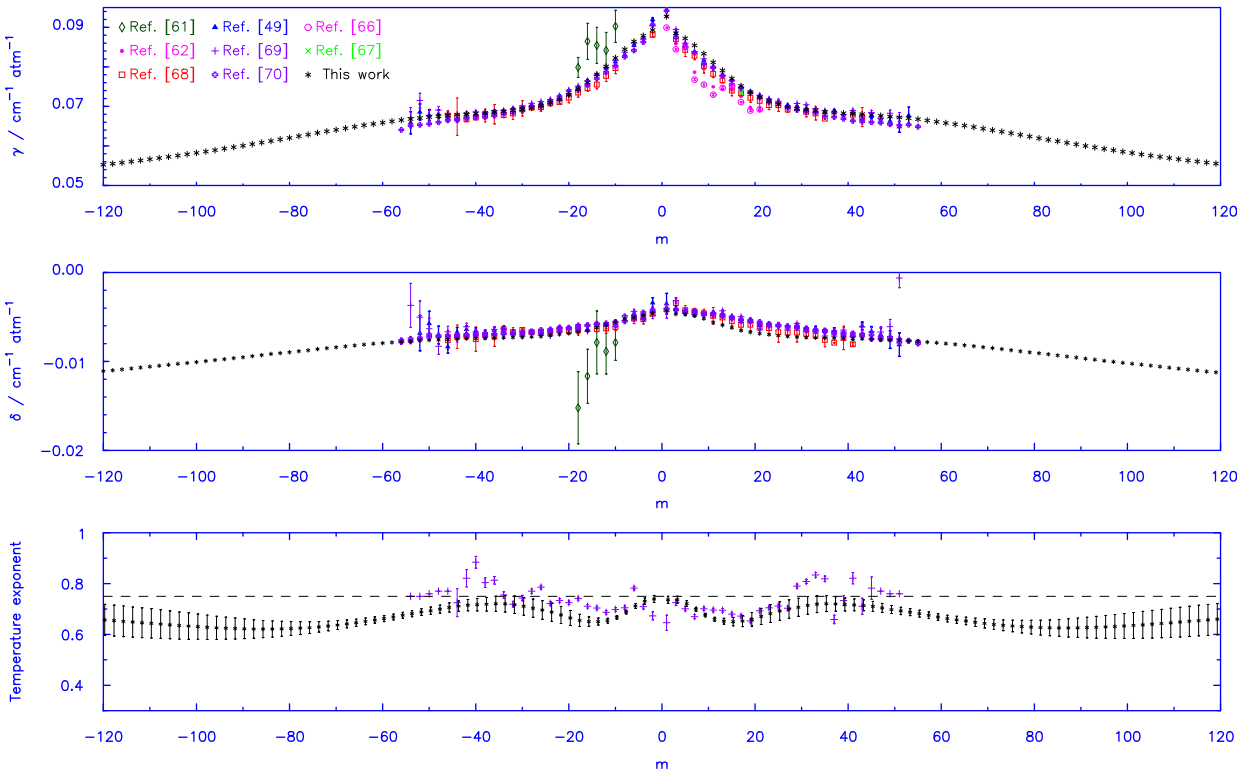

Fig. 6. Final CRB calculations for transitions in the 30012←00001 band of CO_2 broadened by air at $T=296$ K and measurements versus m. Top panel half-widths (in cm^{-1} atm^{-1}) versus m, middle panel line shifts (in cm^{-1} atm^{-1}) versus m, bottom panel temperature exponent of the half-widths versus m.

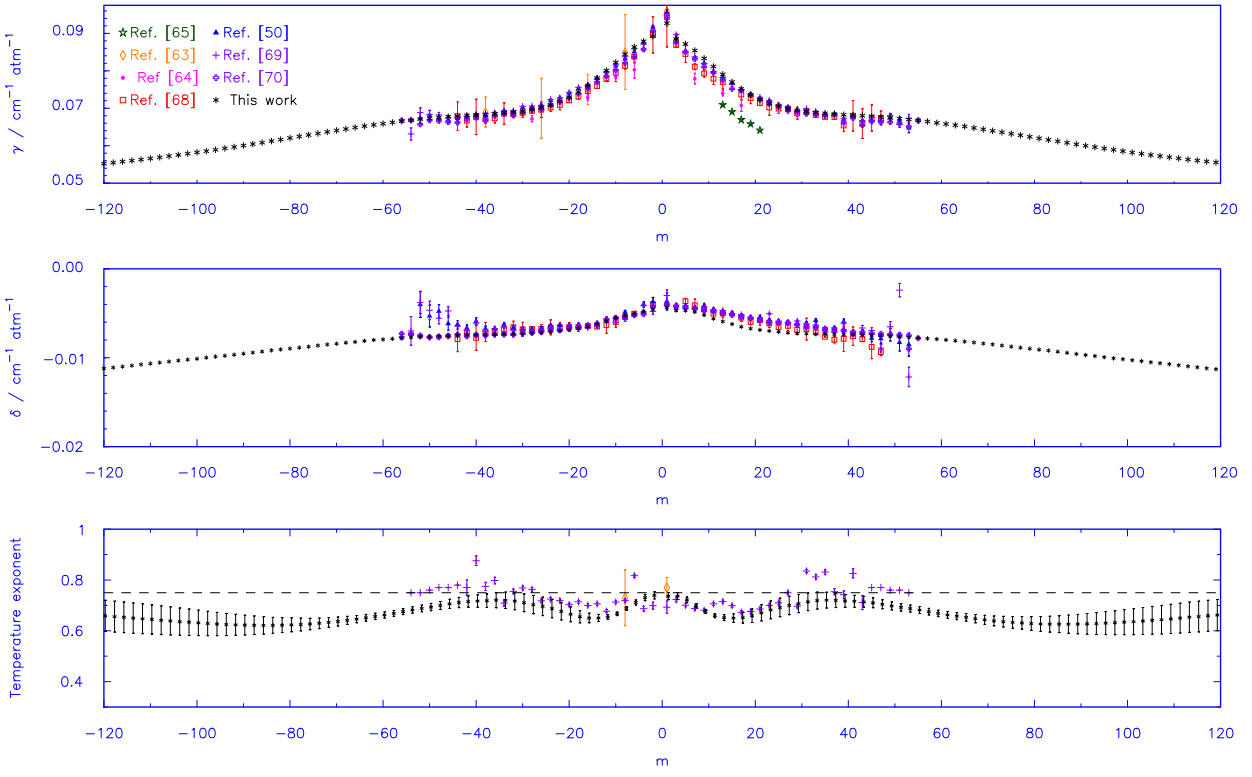

Fig. 7. Final CRB calculations for transitions in the 30013←00001 band of CO_2 broadened by air at $T=296$ K and measurements versus m. Top panel half-widths (in cm^{-1} atm^{-1}) versus m, middle panel line shifts (in cm^{-1} atm^{-1}) versus m, bottom panel temperature exponent of the half-widths versus m.

Table 6
Statistics for the comparison of the calculations to measurement for CO_2-air.

Parameter	Reference	No. of data	APD	SD
30012←00001				
γ	[61]	5	8.24	2.64
	[66]	11	−6.24	3.32
	[62]	11	−4.60	2.57
	[68]	38	−1.65	1.22
	[49]	54	−0.1	1.27
	[70]	56	−1.45	1.21
	[69]	53	0.41	1.36
	[67]	1	−2.21	
n	[69]	53	5.30	6.29
	Reference	No. of data	AD†	$S\tilde{D}$†
δ	[61]	5	−0.0041	0.0028
	[68]	41	0.00031	0.00045
	[49]	52	0.00063	0.00052
	[70]	56	0.00051	0.00036
	[69]	53	0.00080	0.0012
30013←00001				
γ	[50]	53	−0.16	1.25
	[70]	56	−1.24	1.18
	[69]	54	−0.02	1.46
	[68]	44	−1.66	1.53
	[65]	5	−12.04	0.55
	[64]	10	−4.58	3.11
	[63]	5	0.66	1.80
n	[69]	54	5.58	5.18
	[63]	2	5.07	–
	Reference	No. of data	AD†	$S\tilde{D}$†
δ	[50]	53	0.00079	0.00077
	[68]	42	0.00020	0.00062
	[70]	56	0.00032	0.00048
	[69]	54	0.00076	0.0013

† see text for definitions of AD and $S\tilde{D}$.

For half-widths in the 30013←00001 band, the agreement between CRB calculations with the measurements of Devi et al. [50], Toth et al. [68], and Predoi-Cross et al. [69,70], and Nakamichi et al. [63] are very good with |APD|s from 0 to 1.7 and standard deviations from 1.25 to 1.80%. Comparison with the measurements of Hikida and Yamada [64] is not as good APD = −4.58 and a SD of about 3%, however they have modeled the profile with a Galatry profile. Comparison with the 5 measurements of Pouchet et al. [65] show an excellent standard deviation, 0.55, but the measurements are shifted down from the calculations and other measurements by about 12 percent. For the line shifts, the agreement of the calculations with the measurements of Toth et al. [68] and Predoi-Cross et al. [70] is quite good, roughly $2–3\times10^{-4}$ cm^{-1} atm^{-1} with $S\tilde{D}$ around $5–6\times10^{-4}$ cm^{-1} atm^{-1}. Comparison with the line shift measurements of Devi et al. [50] are not as good with an AD of 0.00079 cm^{-1} atm^{-1} and $S\tilde{D}$ of 0.00077 cm^{-1} atm^{-1}. The comparison of the calculated temperature exponents with the measurements of Predoi-Cross et al. [69] and Nakamichi et al. [63] shows good agreement. The statistics for these comparisons are presented in Table 6.

5. Conclusions

In this study, the complex Robert–Bonamy formalism was used to calculate the half-width, its temperature dependence, and the line shift for CO_2 perturbed by O_2 and air for transitions in two of the Fermi tetrad bands; 30012←00001 and 30013←00001. The results show almost no vibrational dependence with the γ, δ, and n values being identical in both bands to within the estimated uncertainty. Parameters describing the intermolecular potential that are not well known were adjusted to fit the three line shape parameters simultaneously. As in the study of part I, it was found that the results are very sensitive to the intermolecular potential. The calculations require that the atom–atom component of the intermolecular potential be expanded to high *order* and *rank*, that the imaginary components of the theory are included, and that the trajectories are determined using Hamilton's equations. The comparison of the calculated values with measured values reported in the literature for both O_2-, and air-broadening shows very good agreement. The calculations allow a determination of the line shape parameters for large values of J, which is important for the line mixing problem [71]. Having a physically correct intermolecular potential will allow the vibrational dependence of the line shape parameters to be studied as well. The data in Tables 3 and 5, as well as the results for the 30013←00001 band can be obtained at the web site of one of the authors; faculty.uml.edu/Robert_Gamache.

Acknowledgment

JL, RRG, ALL are pleased to acknowledge support of this research by the National Science Foundation through Grant No. ATM-0803135. Any opinions, findings, and conclusions or recommendations expressed in this material are those of the author(s) and do not necessarily reflect the views of the National Science Foundation. RRG and JMH are also grateful to the Paris-Est *Pôle de Recherche et d'Enseignement Supérieur* who provided a one month research scientist position for RRG at LISA in June 2011.

Appendix A. Supplementary materials

Supplementary data associated with this article can be found in the online version at doi:10.1016/j.jqsrt.2012.02.015.

References

[1] Gamache RR, Lamouroux J, Laraia AL, Hartmann J-M, Boulet C. Semiclassical calculations of half-widths and line shifts for transitions in the 30012←00001 and 30013←00001 bands of CO_2 I: collisions with N_2. J Quant Spectrosc Radiat Transfer, doi:10.1016/j.jqsrt.2012.02.014, this issue.
[2] Rothman LS, Jacquemart D, Barbe A, Benner DC, Birk M, Brown LR, et al. The HITRAN 2004 molecular spectroscopic database. J. Quant. Spectrosc. Radiat. Transfer 2005;96:139–204.
[3] Toth RA, Brown LR, Miller CE, Malathy Devi V, Benner DC. Spectroscopic database of CO_2 line parameters: 4300–7000 cm^{-1}. J. Quant. Spectrosc. Radiat. Transfer 2008;109:906–21.
[4] Crisp D, Atlas RM, Breon F-M, Brown LR, Burrows JP, Ciais P, et al. The orbiting carbon observatory (OCO) mission. Adv. Space Res. 2004;34:700–9.

[5] Crisp D, Miller C. The need for atmospheric carbon dioxide measurements from space: Contributions from a Rapid Reflight of the Orbiting Carbon Observatory. 〈http://www.nasa.gov/pdf/363474main_OCO_Reflight.pdf〉. 2009, Jet Propulsion Laboratory: Pasadena.

[6] Inoue G, Yokota T, Oguma H, Higurashi A, Morino I, Aoki T. Overview of greenhouse gases observing satellite (GOSAT) of Japan, AGU 2004 Fall Meeting, San Francisco, California, USA, 2004.

[7] Bovensmann H, Buchwitz M, Burrows JP, Reuter M, Krings T, Gerilowski K, et al. A remote sensing technique for global monitoring of power plant CO_2 emissions from space and related applications. Atmos. Meas. Tech. 2010;3:781–811.

[8] Drossart P, Piccioni G, Adriani A, Angrilli F, Arnold G, Baines KH, et al. Scientific goals for the observation of Venus by VIRTIS on ESA/Venus express mission, Planet. Space Sci. 2007;55:1653–72.

[9] Fedorova A, Korablev O, Bertaux J-L, Rodin A, Kiselev A, Perrier S. Mars water vapor abundance from SPICAM IR spectrometer: seasonal and geographic distributions. J. Geophys. Res. 2006;111:E09S8.

[10] McCleese DJ, Schofield JT, Taylor FW, Calcutt SB, Foote MC, Kass DM, et al. Mars climate sounder: an investigation of thermal and water vapor structure, dust and condensate distributions in the atmosphere, and energy balance of the polar regions. J. Geophys. Res. 2007;112:E05S6.

[11] Wunch D, Toon GC, Blavier J-FL, Washenfelder RA, Notholt J, Connor BJ, et al. The total carbon column observing network (TCCON). Philos. Trans. R. Soc. A 2011;369:2087–112.

[12] Robert D, Bonamy J. Short range force effects in semiclassical molecular line broadening calculations. J. Phys. France 1979;40:923–43.

[13] Anderson PW. Dissertation Physics. Harvard University; 1949.

[14] Anderson PW. Pressure broadening in the microwave and Infra-Red regions. Phys. Rev. 1949;76:647–61.

[15] Tsao CJ, Curnutte B. Line-widths of pressure-broadened spectral lines. J. Quant. Spectrosc. Radiat. Transfer 1962;2:41–91.

[16] Davies RW. Many-body treatment of pressure shifts associated with Collisional broadening. Phys. Rev. A 1975;12:927–46.

[17] Davies RW, Oli BA. Theoretical calculations of H_2O linewidths and pressure shifts: comparison of the Anderson theory with quantum many-body theory for N_2 and air-broadened lines. J. Quant. Spectrosc. Radiat. Transfer 1978;20:95–120.

[18] Tipping RH. Impact theory for the noble gas pressure-induced line widths and shifts of HCl spectral lines. Ph.D. Dissertation, Department of Physics, The Pennsylvania State University, 1969.

[19] Tipping RH, Herman RM. Impact theory for the noble gas pressure-induced HCl vibration–rotation and pure rotation line widths – I. J. Quant. Spectrosc. Radiat. Transfer 1970;10:881–96.

[20] Herman RM, Tipping RH. Impact theory for the noble gas pressure-induced HCl vibration–rotation and pure rotation line shifts – II. J. Quant. Spectrosc. Radiat. Transfer 1970;10:897–908.

[21] Neilsen WB, Gordon RG. On a semiclassical study of molecular collisions. I. General method. J. Chem. Phys. 1973;58:4131–6.

[22] Kubo R. Generalized cumulant expansion method. J. Phys. Soc. Jpn. 1962;17:1100–20.

[23] Neshyba SP, Lynch R, Gamache RR, Gabard T, Champion J-P. Pressure induced widths and shifts for the v_3 band of methane. J. Chem. Phys. 1994;101:9412–21.

[24] Labani B, Bonamy J, Robert D, Hartmann J-M, Taine J. Collisional broadening of rotation–vibration lines for asymmetric top molecules I. Theoretical model for both distant and close collisions. J. Chem. Phys. 1986;84:4256–67.

[25] Hartmann J-M, Camy-Peyret C, Flaud J-M, Bonamy J, Robert D. New accurate calculations of ozone line-broadening by O_2 and N_2. J. Quant. Spectrosc. Radiat. Transfer 1988;40:489–95.

[26] Antony B, Gamache P, Szembek C, Niles D, Gamache RR. Modified complex Robert–Bonamy formalism calculations for strong to weak interacting systems. Mol. Phys. 2006;104:2791–9.

[27] Lynch R. Half-widths and line shifts of water vapor perturbed by both nitrogen and oxygen. Ph.D. dissertation, Physics Department, University of Massachusetts Lowell, 1995.

[28] Lynch R, Gamache RR, Neshyba SP. Fully complex implementation of the Robert–Bonamy formalism: halfwidths and line shifts of H_2O broadened by N_2. J. Chem. Phys. 1996;105:5711–21.

[29] Gamache RR, Lynch R, Plateaux JJ, Barbe A. Halfwidths and line shifts of water vapor broadened by CO_2: measurements and complex Robert–Bonamy formalism calculations. J. Quant. Spectrosc. Radiat. Transfer 1997;57:485–96.

[30] Lamouroux J, Gamache RR, Laraia AL, Ma Q, Tipping RH. Comparison of trajectory models in calculations of N_2-broadened half-widths and N_2-induced line shifts for the rotational band of $H_2^{16}O$ and comparison with measurements. J Quant Spectrosc Radiat Transfer, doi:10.1016/j.jqsrt.2011.11.010, this issue.

[31] Jones JE. On the determination of molecular fields.II. From the equation of state of a gas. Proc. R. Soc. A 1924;106:463–77.

[32] Hirschfelder JO, Curtiss CF, Bird RB. Molecular Theory of Gases and Liquids. New York: Wiley; 1964.

[33] Diaz Pena M, Pando C, JAR Renuncio. Combination rules for intermolecular potential parameters. I. Rules based on approximations for the long-range dispersion energy. J. Chem. Phys. 1982;76:325–32.

[34] Diaz Pena M, Pando C, JAR Renuncio. Combination rules for intermolecular potential parameters. II. Rules based on approximations for the long-range dispersion energy and an atomic distortion model for the repulsive interactions. J. Chem. Phys. 1982;76:333–9.

[35] Good RJ, Hope CJ. Test of combining rules for intermolecular distances. Potential function constants from second virial coefficients. J. Chem. Phys. 1971;55:111–6.

[36] Gamache RR, Fischer J. Half-widths of $H_2^{16}O$, $H_2^{18}O$, $H_2^{17}O$, $HD^{16}O$, and $D_2^{16}O$: I Comparison between Isotopomers. J. Quant. Spectrosc. Radiat. Transfer 2003;78:289–304.

[37] Gamache RR. Line shape parameters for water vapor in the 3.2 to 17.76 μm region for atmospheric applications. J. Mol. Spectrosc. 2005;229:9–18.

[38] Gamache RR, Hartmann J-M. Collisional parameters of H_2O lines: effects of vibration. J. Quant. Spectrosc. Radiat. Transfer 2004;83:119–47.

[39] Gray CG, Gubbins KE. Theory of Molecular Fluids. Oxford: Clarendon Press; 1984.

[40] Sack RA. Two-center expansion for the powers of the distance between two points. J. Math. Phys. 1964;5:260–8.

[41] Neshyba SP, Gamache RR. Improved line broadening coefficients for asymmetric rotor molecules: application to ozone perturbed by nitrogen. J. Quant. Spectrosc. Radiat. Transfer 1993;50:443–53.

[42] Bose TK, Cole RH. Dielectric and pressure virial coefficients of imperfect gases. II. CO_2–argon mixtures. J. Chem. Phys. 1970;52:140–7.

[43] Tanaka Y, Jursa AS, LeBlanc FJ. Higher ionization potentials of linear triatomic molecules. I. CO_2. J. Chem. Phys. 1960;32:1199–205.

[44] Stogryn DE, Stogryn AP. Molecular multipole moments. Mol. Phys. 1966;11:371–93.

[45] Bogaard MP, Orr BJ. In: Buckingham, A.D., Ed. MPT International Review of Science, Physical Chemistry, Series Two, Vol. 2. Molecular Structure and Properties, Butterworths, London (Chapter 5) 1975.

[46] Lamouroux J, Gamache RR, Laraia AL, Hartmann J-M, Boulet C. Semiclassical calculations of half-widths and line shifts for transitions in the $30012 \leftarrow 00001$ and $30013 \leftarrow 00001$ bands of CO_2 III: self collisions, Submitted to J. Quant. Spectrosc. Radiat. Transfer 2012.

[47] Graham C, Pierrus J, Raab RE. Measurements of the electric quadrupole moments of CO_2, CO and N_2. Mol. Phys. 1989;67:939–55.

[48] Miller CE, Brown LR. Near infrared spectroscopy of carbon dioxide I. $^{16}O^{12}C^{16}O$ line positions. J. Mol. Spectrosc. 2004;228:329–54.

[49] Devi VM, Benner DC, Brown LR, Miller CE, Toth RA. Line mixing and speed dependence in CO_2 at 6348 cm^{-1}: positions, intensities, and air- and self-broadening derived with constrained multispectrum analysis. J. Mol. Spectrosc. 2007;242:90–117.

[50] Devi VM, Benner DC, Brown LR, Miller CE, Toth RA. Line mixing and speed dependence in CO_2 at 6227.9 cm^{-1}: constrained multispectrum analysis of intensities and line shapes in the $30013 \leftarrow 00001$ band. J. Mol. Spectrosc. 2007;245:52–80.

[51] Huber KP, Herzberg G. Molecular Spectra and Molecular Structure: Constants of Diatomic Molecules. New York: Van Nostrand; 1979.

[52] Herzberg G. Molecular Spectra and Molecular Structure II. Infrared and Raman Spectra of Polyatomic Molecules. New Jersey.D. Van Nostrand Company, Inc.; 1960.

[53] Gamache RR. Analytical evaluation of the Maxwell–Boltzmann velocity average in pressure-broadened half-width calculations. J. Mol. Spectrosc. 2001;208:79–86.

[54] Tran H, Bermejo D, Domenech J-L, Joubert P, Gamache RR, Hartmann J-M. Collisional parameters of H_2O lines: velocity effects on the line shape. J. Quant. Spectrosc. Radiat. Transfer 2007;108:126–45.

[55] Barbe A. Workshop Proceedings, Atmospheric Spectroscopy Applications Workshop, ASA REIMS 96, Université de Reims Champagne Ardenne, 1996.

[56] Smith MAH. editor, NASA Conference Publication 2396, NASA, 1985.

[57] Smith MAH. editor., Third Langley Spectroscopic Parameters Workshop, NASA Langley Research Center, Hampton, VA, 1992.

[58] Bouanich J-P. Site–Site Lennard-Jones potential parameters for N_2, O_2, H_2, CO and CO_2. J. Quant. Spectrosc. Radiat. Transfer 1992;47: 243–50.
[59] Devi VM, Benner DC, Miller CE, Predoi-Cross A. Lorentz half-width, pressure-induced shift and speed-dependent coefficients in oxygen-broadened CO_2 bands at 6227 and 6348 cm^{-1} using a constrained multispectrum analysis. J. Quant. Spectrosc. Radiat. Transfer 2010;111:2355–69.
[60] Birnbaum G. Microwave pressure broadening and its application to intermolecular forces. Adv. Chem. Phys. 1967;12:487–548.
[61] De Rosa M, Corsi C, Gabrysch M, D'Amato F. Collisional broadening and shift of lines in the $2\nu_1+2\nu_2+\nu_3$ band of CO_2. J. Quant. Spectrosc. Radiat. Transfer 1999;61:97–104.
[62] Li JS, Liu K, Zhang WJ, Chen WD, Gao XM. Self-, N_2- and O_2-broadening coefficients for the $^{12}C^{16}O_2$ transitions near-IR measured by a diode laser photoacoustic spectrometer. J. Mol. Spectrosc. 2008;252:9–16.
[63] Nakamichi S, Kawaguchi Y, Fukuda H, Enami S, Hashimoto S, Kawasaki M, et al. Buffer-gas pressure broadening for the $(30^0\ 1)_{III}\leftarrow(0\ 0\ 0)$ band of CO_2 measured with continuous-wave cavity ring-down spectroscopy. Phys. Chem. Chem. Phys. 2006;8:364–8.
[64] Hikida T, Yamada KMT. N_2- and O_2-broadening of CO_2 for the $(30^01)_{III}\leftarrow(00^00)$ band at 6231 cm^{-1}. J. Mol. Spectrosc. 2006;239: 154–9.
[65] Pouchet I, Zéninari V, Parvitte B, Durry G. Diode laser spectroscopy of CO_2 in the 1.6 μm region for the in situ sensing of the middle atmosphere. J. Quant. Spectrosc. Radiat. Transfer 2004;83:619–28.
[66] Li JS, Liu K, Zhang WJ, Chen WD, Gao XM. Pressure-induced line broadening for the $(30012)\leftarrow(00001)$ band of CO_2 measured with tunable diode laser photoacoustic spectroscopy. J. Quant. Spectrosc. Radiat. Transfer 2008;109:1575–85.
[67] Long DA, Bielska K, Lisak D, Havey DK, Okumura M, Miller CE, et al. The air-broadened, near-infrared CO_2 line shape in the spectrally isolated regime: evidence of simultaneous dicke narrowing and speed dependence. J. Chem. Phys. 2011;135:064308.
[68] Toth RA, Miller CE, Devi VM, Benner DC, Brown LR. Air-broadened halfwidth and pressure shift coefficients of $^{12}C^{16}O_2$ bands: 4750–7000 cm^{-1}. J. Mol. Spectrosc. 2007;246:133–57.
[69] Predoi-Cross A, McKellar ARW, Benner DC, Devi VM, Gamache RR, Miller CE, et al. Temperature dependences for air-broadened Lorentz half-width and pressure shift coefficients in the $30013\leftarrow00001$ and $30012\leftarrow00001$ bands of CO_2 near 1600 nm. Can. J. Phys. 2009;87:517–35.
[70] Predoi-Cross A, Liu W, Holladay C, Unni AV, Schofield I, McKellar ARW, et al. Line profile study of transitions in the $30012\leftarrow00001$ and $30013\leftarrow00001$ bands of carbon dioxide perturbed by air. J. Mol. Spectrosc. 2007;246:98–112.
[71] Lamouroux J, Tran H, Laraia AL, Gamache RR, Rothman LS, Gordon IE, et al. Updated database plus software for line-mixing in CO_2 infrared spectra and their test using laboratory spectra in the 1.5–2.3 μm region. J. Quant. Spectrosc. Radiat. Transfer 2010;111:2321–31.